

# Multifractal characteristics of external anal sphincter based on sEMG signals

Paulina Trybek<sup>1\*</sup>, Michal Nowakowski<sup>2</sup>, Lukasz Machura<sup>1</sup>,

<sup>1</sup> Division of Computational Physics and Electronics, Institute of Physics, Silesian Center for Education and Interdisciplinary Research, University of Silesia, Chorzow, Poland

<sup>2</sup> Department of Medical Education, Jagiellonian University Medical College, Krakow, Poland

\* paulina.trybek@smcebi.edu.pl

## Abstract

This work presents the application of Multifractal Detrended Fluctuation Analysis for the surface electromyography signals obtained from the patients suffering from rectal cancer. The electrical activity of an external anal sphincter at different levels of medical treatment is considered. The results from standard MF DFA and the EMD-based MF DFA method are compared. Two distinct scaling regions were identified. Within the region of short time scales the calculated spectra exhibit the shift towards higher values of the singularity exponent for both methods. In addition obtained spectra are shifted towards the lower values of singularity exponent for the EMD-based MF DFA.

## 1 Introduction

Over last few decades a surface electromyography due to its non-invasive character has gained a wide range of applications in the field of examination of a neuromuscular system. This work is focused on quite a unique application of the sEMG concerning a diagnosis of anal sphincter of the patients suffering from a rectal cancer [1, 2]. Rectal cancer remains to be one of the most frequent cancers in humans [3]. It requires complex multimodal treatment composed of surgery, irradiation and chemotherapy. All those methods can cause significant stool continence related problems hence proper assessment of anorectal innervation before and after the treatment can be crucial for prevention and treatment of complications. sEMG enables non-invasive monitoring of the anal sphincter function [4, 5, 6] and is a very promising method of testing of innervation of muscles. Since innervation deficits are one of suggested mechanisms for severe treatment related complications in up to 40% of rectal cancer patients development of proper innervation assessment methodology is crucial. Proper evaluation of sEMG signals remains to be a significant problem inhibiting diagnostic potential of this methodology. Our analysis is focused on the signals recorded from the external anal sphincter. The electrical activity of this specific muscle group is frequently investigated in the context of the patients with defecation disorders [7].

Regardless the application, sEMG always represents highly complex signal with a low signal to noise ratio [8]. The nonlinearity of sEMG data has been investigated in recent years [9] and great effort has been devoted to the application the variety of nonlinear methods. Traditional analysis, mainly based on the conventional statistical tests of mean, median or frequency components brings only limited knowledge on the actual process hidden behind the acquired data.

In the last few years there has been a growing interest in fractal properties of physiological data, also in the context of sEMG signals [10, 11, 12]. This work propose the application of the modified Detrended Fluctuation Analysis (MF DFA) based on Empirical Mode Decomposition (EMD) to the sEMG signals. The EMD and MF DFA techniques can be used to trace out the features of non-linear and non-stationary signals. Moreover both methods have a broad spectrum of applications individually. MF DFA, developed by Kantelhardt et al. [13] has been used in many disciplines and still attracts considerable attention in the field of physiology, economy, climatology, to name but a few. In relation to the electrophysiological signals, MF DFA brought a significant contribution to the analysis of heart rate variability [14, 15]. For the Empirical Mode Decomposition (EMD) the equally wide range of applications can be found, such as the removal of artifacts and noise reduction from the signals [16]. EMD also exhibits better results in the process of detrending in comparison for example with the typically used least square method [17]. This aspect has been used in the modified detrending algorithm which is presented in this paper. The use of the EMD method in the context of detrending operation results in a more accurate trend, which is not predetermined, and therefore is closely related to the nature of real data [18].

Moreover it is documented in literature that this approach outperforms standard MF DFA for large fluctuations [19].

The paper is organized as follows. Section 2 presents both detrending methods and a multifractal formalism for data analysis. Next section 3 describes the experimental data. The results are presented in Section 4. The last section summarizes the results and draws conclusions.

## 2 Method

### 2.1 DFA

DFA method was first proposed by Peng in 1994 for investigating the correlation in DNA structure [20]. The last years have seen a renewed importance in application of the method to the biological data, also for distinguish healthy and pathological states [21]. The basic idea of this technique relies on the assumption that signal is influenced by the short-term and long-term features. For the proper interpretation of effects hidden behind internal dynamics the signal is analyzed at multiple scales [22]. The brief description of the original DFA algorithm is presented below.

The procedure starts with calculation of the profile  $y_i$  as the cumulative sum of the data  $x_i$  with the subtracted mean  $\langle x \rangle$ :

$$y_i = \sum_{k=1}^i [x_k - \langle x \rangle] \quad (1)$$

Next, the cumulative signal  $y_i$  is split into  $N_s$  equal non-overlapping segments of size  $s$ . Here for the length  $s$  of the segments we use powers of two,  $s = 2^r, r = 4 \dots 11$ . For all segments  $v = 1, \dots, N_s$  the local trend  $y_{v,i}^m$  is calculated. In a standard DFA method the trend is calculated by means of the least-square fit of order  $m$ . In this work  $m = 2$  was used. The variance  $F^2$  as a function of the segment length  $s$  is calculated for each segment  $v$  separately.

$$F^2(s, v) \equiv \frac{1}{s} \sum_{i=1}^s (y_{v,i}^m - y_{v,i})^2. \quad (2)$$

For the last step the Hurst scaling exponent  $H$  is calculated as the slope of the regression line of double-logarithmic dependence,  $\log F \sim H \log s$ .

### 2.2 Empirical Mode Decomposition (EMD)

The EMD is an iterative technique which decomposes the signal  $x(t)$  into finite number of Intrinsic Mode Functions (IMFs)  $c_i(t)$ . The final residual  $r_n(t)$  can be interpreted as an actual trend.

$$x(t) = \sum_{i=1}^n c_i(t) + r_n(t) \quad (3)$$

The calculated signal must satisfy two conditions in order to be IMF: (i) the number of extrema and the number of zero crossing must be equal or differ at most by one; and (ii) the mean value of the upper and lower envelope defined by local maxima and minima must be zero. The standard EMD method often faces some difficulties, which are recurrently the consequence of signal intermittency referred to as Mode Mixing problem. Ensemble Empirical Mode Decomposition (EEMD) [23] and more recent Complete Ensemble Empirical Mode Decomposition (CEEMD) [24] have been proposed in order to overcome this complication. Both methods are based on the averaging over several realisations of Gaussian white noise artificially added to the original signal. For this work, however, we use only standard EMD due to the fact that only residual  $r_n$ , i.e. the data trend, is needed for further calculations and none of the individual IMFs are considered here explicitly.

### 2.3 EMD based DFA

Our analysis was branched into standard DFA algorithm and non-standard one based on EMD technique. The former method uses the least-square estimation of the order  $m$ . The latter utilizes the fact that the residual  $r_n$  (3) represents the local trend, thus the standard polynomial fit (DFA) can be replaced by a residuum for each segment [25]. An example of local trends calculated with both methods is presented on Fig.1 for the segment size  $s = 64$ . The slight differences between solid black and red lines, which represent DFA and EMD method, respectively, influence the further results.

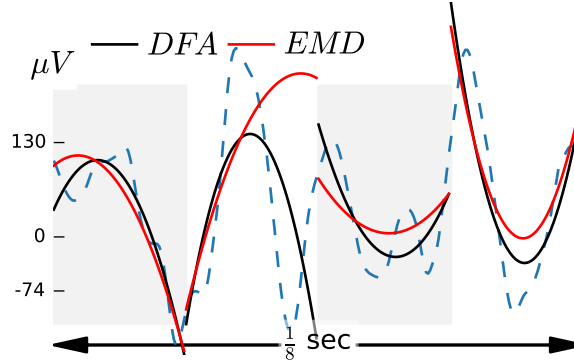


Figure 1: Two detrending methods: DFA (solid black) and EMD (solid red) are presented for the profile  $y_i$  of the sEMG example data (dashed blue).

## 2.4 MF DFA

MF DFA is based on the scaling properties of the fluctuations. The brief description of the method is presented below, however, for the detailed specification we suggest works by Kantelhardt et al. [13, 26], Ihlen [27] or Salat et al. [28]. In order to extend the monofractal DFA (2.1) to the multifractal DFA it is necessary to indicate the  $q^{th}$  statistical moment of the calculated variance (2). The equations that describe the fluctuation functions are presented below.

$$F_q(s) = \begin{cases} \left( \frac{1}{2N_s} \sum_{v=1}^{2N_s} [F^2(s, v)]^{\frac{q}{2}} \right)^{\frac{1}{q}}, & q \neq 0, \\ \exp \left\{ \frac{1}{4N_s} \sum_{v=1}^{2N_s} \ln [F^2(s, v)] \right\}, & q = 0. \end{cases} \quad (4)$$

Next, the determination of the scaling law  $F_q(s) \sim s^{h(q)}$  of the fluctuation function (4) is performed with the use of the log-log dependencies of  $F_q(s)$  versus segment sizes  $s$  for all values of  $q$  separately. The  $q$ -order Hurst exponent  $h(q)$  is required in order to calculate the further dependencies. The mass exponent is obtained via the formula

$$\tau(q) = qh(q) - 1. \quad (5)$$

It is then used to calculate a  $q$ -order singularity Hölder exponent  $\alpha = \tau'(q)$  where the prime means differentiation with respect to the argument. In turn the  $q$ -order singularity dimension can be constructed

$$f(\alpha) = q\alpha - \tau(q) = q[\alpha - h(q)] + 1. \quad (6)$$

The singularity dimension  $f(\alpha)$  is related to the mass exponent  $\tau(q)$  by a Legendre transform. The multifractal spectrum, i.e. the dependence  $f(\alpha)$  vs  $\alpha$  is the final result of MF DFA method.

## 3 Material

### 3.1 sEMG signal source

Data acquisition system consists of anal probe developed at Laboratory of Engineering of Neuromuscular System and Motor Rehabilitation of Politecnico di Torino in collaboration with the company OT-Bioelettronica. Signals were obtained from 16 pairs of silver bar electrodes of length 9 mm and width 1 mm each. Electrodes were separated by 8 mm and arranged concentrically at three levels 35–44 mm, 18–27 mm and around 9 mm of rectal canal depth from the anal verge. The probe worked in conjunction with the standard PC over 12 bit NI DAQ MIO16 E-10 transducer (National Instruments, USA). The sampling frequency was 2048 Hz, which for the 10 seconds of the measurement gave 20480 data points. Low and high pass filters were used at 10 and 50 Hz respectively. This resulted in typical 3dB bandwidth for the ADC. The analyzed time series were recorded at four stages: before the treatment ( $D_1$ ) and one month ( $D_2$ ), six months ( $D_3$ ) and one year ( $D_4$ ) after the surgical procedure. The detailed information about the surgery of the rectal cancer and the role of sEMG for the patient diagnosis can be found in [29].

Measurement protocol included consecutively 1 minute relaxation state, three 10 sec recordings at rest and 1 minute relaxation and then three 10 sec recordings at maximum voluntary contraction (MVC). Each signal was recorded at three levels of anal canal depth, respectively 5cm, 3cm and 1cm. For our calculations signal recorded during voluntary contraction at the depth of 1 cm was used. This specific choice of depth was dictated by the

maximal amplitude of EMG signal resulting from the most superficial localisation of external anal sphincter muscle and the biggest bulk of the muscle at this location. Fig. 2 presents an example of the raw signals at four stages of rectal cancer treatment. For better visualization of the character of waveforms, the narrow range of time scale is presented. The difference in the amplitude values between the state directly after operation ( $D_2$ ) and the rest of states ( $D_1, D_3, D_4$ ) is visible to the naked eye. One month after the operation the values of amplitude are respectively lower in comparison with other stages. The signal used in this work is in fact the averaged signal from the first 3 channels which corresponds to the first three pairs of the electrodes. The nearest neighbours average was performed due to the fact that the placement of the probe in subsequent measurements could be inaccurate. In other words the specific electrodes may not be located exactly the same place at the consecutive measurements after the surgery.

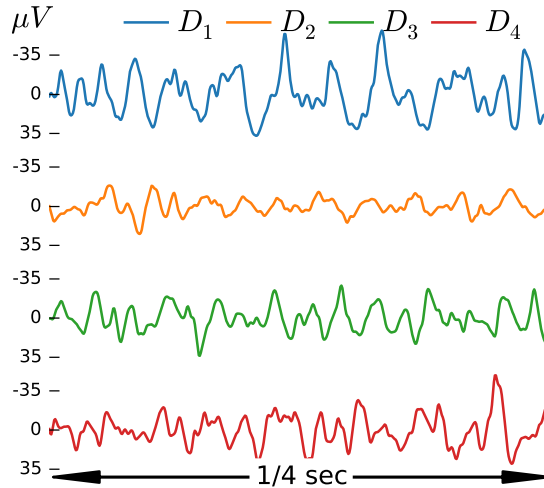


Figure 2: The raw signals truncated to  $1/4$  of the second at four stages of rectal cancer treatment:  $D_1$  is assigned to the state before surgery,  $D_2 - D_4$  correspond to one month, six months and one year after the surgery, respectively.

### 3.2 Patients

The study included 15 subjects, 5 female, age range 46 to 71 (average 53,4 years) and 10 male, age range 40 to 85 (average 62,8 years), diagnosed with rectal cancer and qualified for surgery. Based on localization of rectal cancer patients underwent either Low Anterior Resection (LAR, 9 patients), Anterior Resection (AR, 5 patients) or proctocolectomy (PC, 1 patient).

## 4 Results

### 4.1 Fluctuation Analysis

Clearly, MF DFA is not a black-box method and always requires some individual decisions. First of all, the choice of the scaling range can have a significant impact on the appropriate estimation of the fluctuation function ( $F_q$ ) and consequently the final results [15, 27]. For the calculations presented in this work, the considered range of scales are between  $s \in [2^4, 2^{11}]$ . The parameter  $q$  should consist of positive and negative values in order to detect periods with small and large fluctuations [27]. In our case  $q \in [-5, 5]$  were chosen. A set of  $q$ -order fluctuation functions  $F_q$  vs segment size  $s$  is presented in Fig.3. The two different scale ranges are clearly visible for all  $F_q(s)$  characteristics. This bisection into two distinct scaling regimes plays a crucial role in determination of the  $q$ -order Hurst exponent  $h(q)$  and wherefore impacts the further analysis. The results for DFA and EMD-based detrending method are presented on Fig. 3. Two separate scaling domains was accepted, namely  $s \in [2^4, 2^6]$  and  $s \in [2^8, 2^{11}]$ . Further analysis have been performed for both of this regions separately. The middle values  $s \in (2^6, 2^8)$  are omitted, as there is no clear linear scaling present.

### 4.2 Multifractal spectra

The central result of this work is presented in Fig.4. It sets together the multifractal spectra at all level of treatment process ( $D_1$ - $D_4$ ). The mf-spectrum describes how often the irregularity of certain degree occurs in

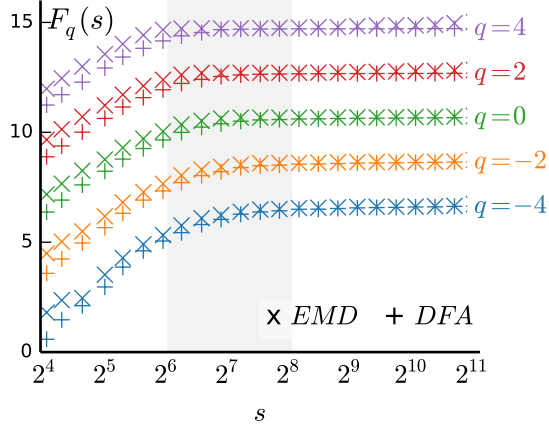


Figure 3:  $q$ -th order fluctuation function (4) with both detrending methods DFA of order 2 and EMD presented for data before the surgery  $D_1$  for selected values of  $q$ . Characteristics were artificially shifted vertically for better visibility.

the signal.  $f(\alpha)$  represent  $q$ -order singularity dimension and  $\alpha$  stands for the  $q$ -order singularity exponent. The typical monofractal time series has dense mf-spectrum around the single point  $(\alpha = 0, f(\alpha) = 1)$ . A large difference between periods when small and large fluctuations takes place increases in turn the width of the spectrum.

There are two general sources of multifractality which can affect the shape of the mf-spectrum: (i) broad probability density function which lies behind the data (or its fluctuations); (ii) different behaviour of the (auto)correlation function for large and small fluctuations; (iii) both situations simultaneously. Simple data shuffling can test the possible source of multifractality. In the case (i) shuffling will not change the mf-spectrum, for (ii) will destroy the effect completely as the shuffling will erase the possible correlations. In the last case (iii) the spectrum will differ from the original one as the shuffled series will exhibit somehow weaker multifractality [30]. The spectra calculated for shuffled data (see black line in Fig. 4) form a tight set of points, significantly shifted towards the lower values of singularity exponent  $\alpha$ , in other words the shuffling operation resulted in a complete destruction of multifractality which occurs for the raw data. Thus it can be concluded that multifractal character of raw data has its cause in different behaviour of the correlation function for large and small fluctuations.

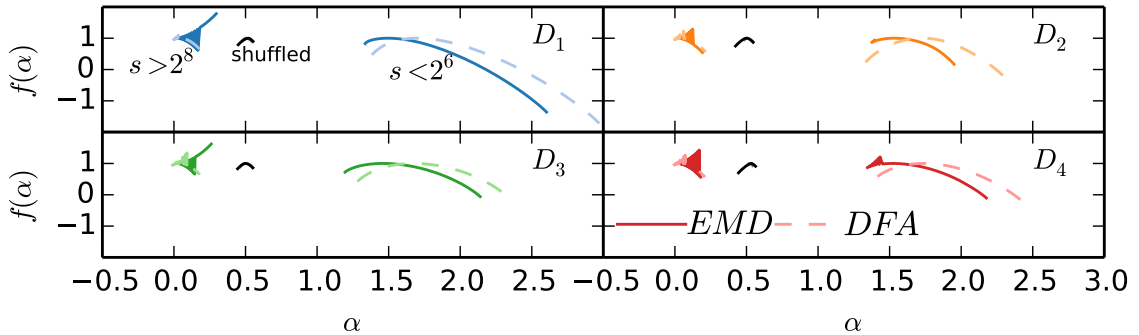


Figure 4: An example of multifractal spectra calculated for one case at four stages of rectal cancer treatment  $D_1 - D_4$ . At each panel three sets of distinct spectra can be found: right which correspond to the scaling region  $s < 2^6$ , the middle panel represent the whole range of scales  $s \in [2^4, 2^{11}]$  after shuffling operation and the left set for  $s > 2^8$ . For each scaling regions two spectra are presented – for the EMD based MF DFA (dark solid lines) and standard MF DFA (light dashed lines). In the case of shuffled data the spectra calculated by both methods are overlapped almost entirely. One can notice the generally found degeneracy of the spectra for  $s > 2^8$  and the shift towards the smaller values of  $\alpha$  for the EMD-based detrending.

For all of the examined cases the relatively wide spectra for the short scales  $s < 2^6$  can be observed. For the large scales  $s > 2^8$  the small set of points located around point  $(0, 1)$  is visible, in that case both multifractal methods result in degenerated narrow spectra for all stages of treatment. This indicates the multifractal character of the sEMG signal for the short scales  $s < 2^6$  and rather monofractal character for the large scales

$s > 2^8$ . For all of the presented analysis, regardless the method, the spectra calculated for small scaling region  $s < 2^6$ , exhibit long right tails, see Fig. 4. It means that the multifractal structure is sensitive to the local fluctuations with small magnitudes on the short time scales only [27]. On the comparison of the spectra obtained by the two methods a shift towards the smaller values of  $\alpha$  (left side) of the spectrum for the small scales  $s < 2^6$  is visible for all signals in the case of the EMD-based MF DFA.

### 4.3 Statistics of spectral parameters

Tab. 1 summarizes the average values of the spectrum width  $\langle \Delta \rangle$  and the specific singularity exponent  $f(\alpha_{max}) = 1$ , which corresponds to the maximum of the spectrum calculated for all of the analyzed cases and the whole set of 16 electrodes at each treatment state.

Table 1: Average values of the spectrum width  $\langle \Delta \rangle$  and maximum of spectrum  $\alpha_{max}$  together with the standard deviations presented for all channels at each state of the treatment  $D_1 - D_4$ . Results are presented for MF DFA and EMD-based MF DFA method.

Average spectrum width $\langle \Delta \rangle$ for $s < 2^6$				
	$D_1$	$D_2$	$D_3$	$D_4$
DFA	0.981 $\pm 0.362$	0.950 $\pm 0.342$	1.053 $\pm 0.418$	0.967 $\pm 0.355$
EMD	0.848 $\pm 0.316$	0.808 $\pm 0.310$	0.880 $\pm 0.350$	0.812 $\pm 0.307$
Average spectrum width $\langle \Delta \rangle$ for $s > 2^8$				
DFA	0.136 $\pm 0.068$	0.142 $\pm 0.052$	0.130 $\pm 0.055$	0.161 $\pm 0.118$
EMD	0.107 $\pm 0.070$	0.112 $\pm 0.053$	0.100 $\pm 0.054$	0.131 $\pm 0.118$
Maximum of the spectrum $\alpha_{max}$ for $s < 2^6$				
DFA	1.580 $\pm 0.107$	1.577 $\pm 0.117$	1.588 $\pm 0.110$	1.593 $\pm 0.104$
EMD	1.405 $\pm 0.098$	1.414 $\pm 0.100$	1.414 $\pm 0.096$	1.423 $\pm 0.089$
Maximum of the spectrum $\alpha_{max}$ for $s > 2^8$				
DFA	0.030 $\pm 0.011$	0.031 $\pm 0.008$	0.031 $\pm 0.012$	0.031 $\pm 0.009$
EMD	0.017 $\pm 0.009$	0.017 $\pm 0.007$	0.017 $\pm 0.010$	0.017 $\pm 0.008$

The location of the maximum of the spectrum is always found for the greater values of the singularity exponent in the case of standard MF DFA method. Also the width of the spectrum is consistently wider for the standard MF DFA. The shift towards the higher values of spectrum parameters for the standard MF DFA is also visible on the presented histograms, see Fig. 5. The differences are more evident in the graphs that characterize the maximum of the spectrum for both small and large range of scales. The normality tests of presented probability distributions by means of the Shapiro–Wilk formula do not allow to reject the hypothesis of normality for some selected cases. At the chosen significance level  $\alpha = 0.05$ ,  $p$ -value is always greater than  $\alpha$  for both the spectrum width and the maximum of spectrum for small scaling range ( $s < 2^6$ ) at the state one month after surgical procedure ( $D_2$ ). Additionally, the same results were obtained for the state one year after the operation ( $D_4$ ), however, for maximum of the spectrum only.

Fig. 6 presents the box plot of spectral parameters calculated for small scaling region  $s < 2^6$ . The comparison of mf-spectrum parameters for different states of treatment show a slight decrease in the average value of the spectrum maximum  $\alpha_{max}$  and spectrum width  $\langle \Delta \rangle$  for the state one month after the surgery –  $D_2$ . The results of the  $p$ -value calculated for nonparametric Wilcoxon test are presented in table 2. The values highlighted in red characterize the statistical significance of the difference between comparing stages. It is noticeable that the results for both methods are ambiguous. In the case of spectrum width, the consistent results are obtained for the state 6 month after surgery ( $D_3$ ). This state differs from all the others at the selected significance level ( $\alpha = 0.05$ ). Considering the result of  $\alpha_{max}$ , the statistically significant difference indicated simultaneously by DFA and EMD occurs between states before and one year after the surgery ( $D_1 - D_4$ ).

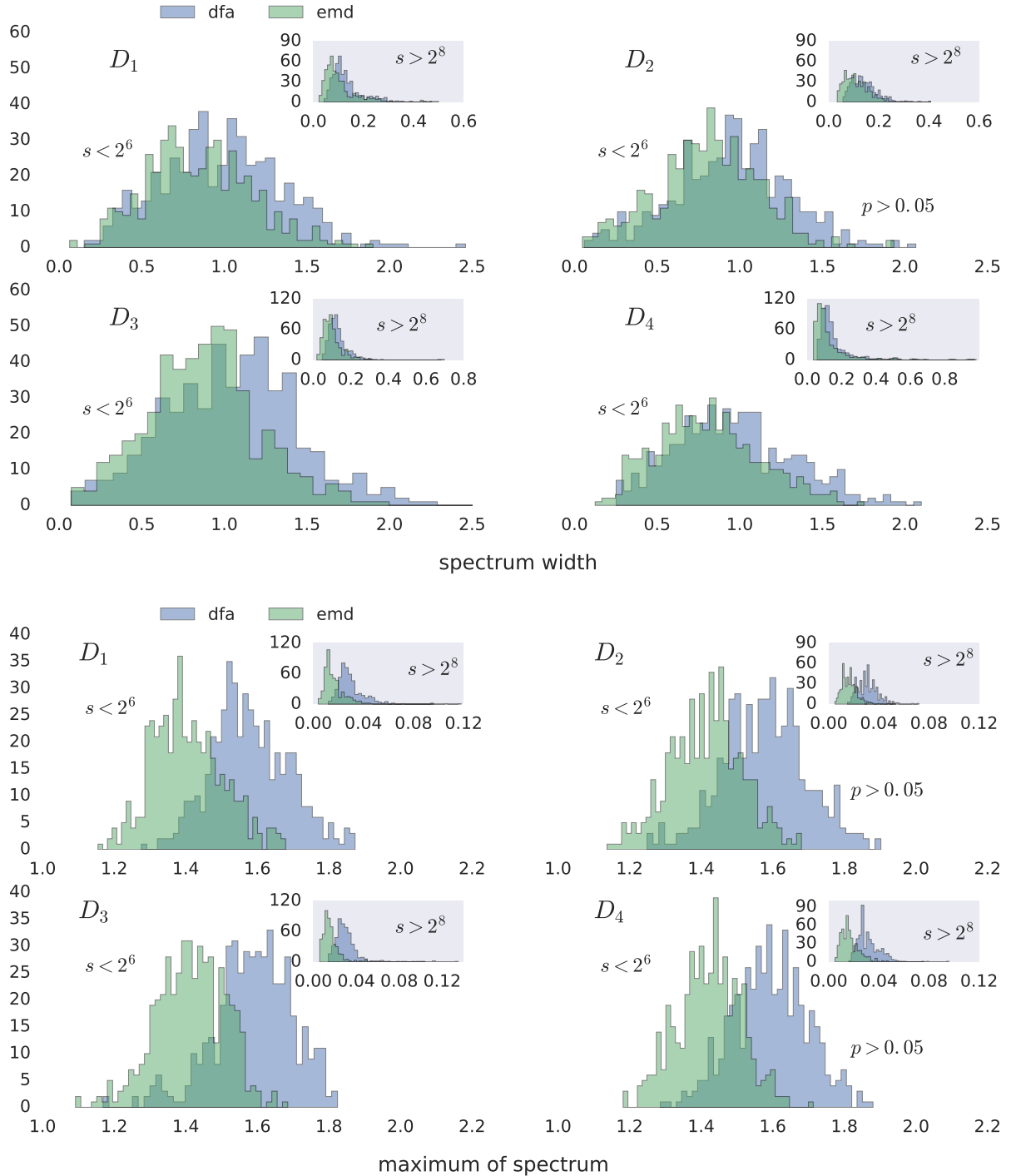


Figure 5: The probability distributions of spectral parameters calculated for both EMD and DFA methods at each state of treatment: large histograms represent the small scaling region  $s < 2^6$ ; the insets stand for the histograms corresponding to the large range of scales.

## 5 Conclusions

This work tests the multifractal character of the sEMG signals recorded from an external anal sphincter at different stages of rectal cancer treatment procedure. For each analyzed time series, two distinct scaling regions were identified, for which multifractal spectra exhibit a different character. The multifractal and monofractal nature can be seen for the regions of short and large time scales respectively. Additionally the multifractal spectra based on standard DFA were compared with EMD based one. The later algorithm shifts the spectra towards the higher fluctuations or smaller values of the singularity exponent. The average values of the considered spectral parameters (width and maximum) for individual stages of treatment are respectively lower in the EMD case. This seems to be the generic behaviour for the analysed EMG data. The changes of parameters

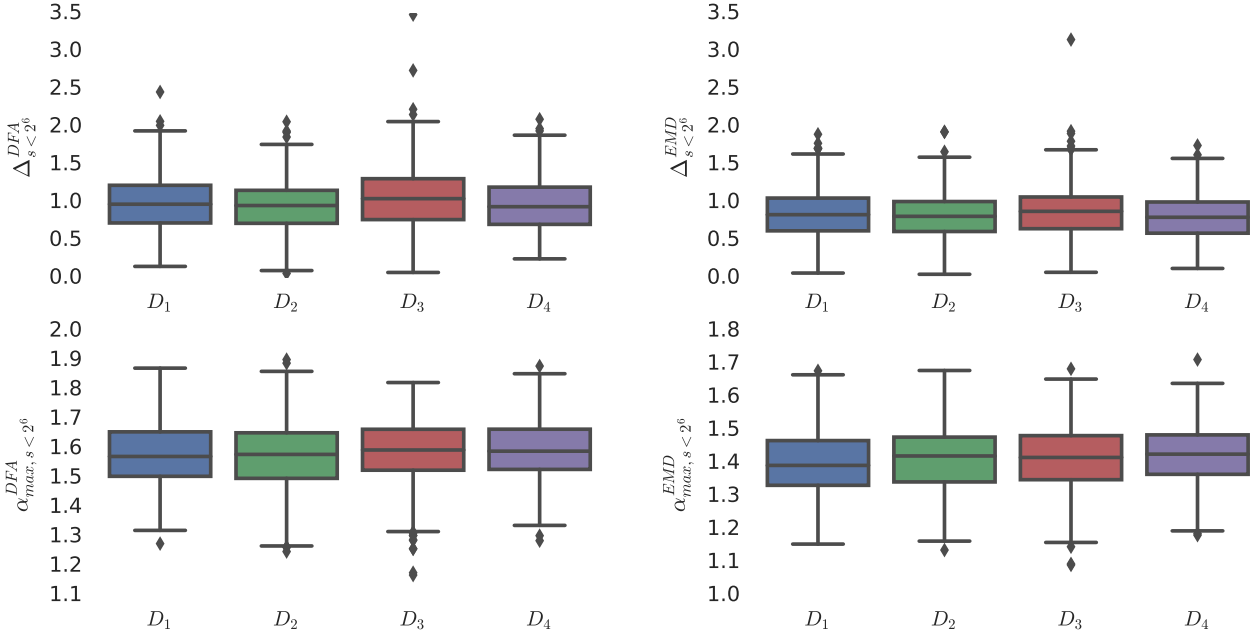


Figure 6: The box plots of spectral parameters calculated for the small range of scales. The box shows the quartiles of the detests whereas points are assigned to outliers values.

Compared stages	spectrum width( $\Delta$ )		maximum of spectrum( $\alpha_{max}$ )	
	DFA	EMD	DFA	EMD
$D_1-D_2$	0.089	0.014	0.881	0.009
$D_1-D_3$	0.001	0.027	0.294	0.337
$D_1-D_4$	0.754	0.031	0.006	0.000
$D_2-D_3$	0.000	0.000	0.007	0.66
$D_2-D_4$	0.341	0.508	0.022	0.424
$D_3-D_4$	0.000	0.000	0.215	0.012

Table 2: The results of  $p$ -value of Wilcoxon Rank test calculated for spectral parameters for a small range of scales.

between individual stages,  $D_1-D_4$  has exactly the same tendency when the results of those two methods are compared. On top of that the source of multifractality within the short time scales was identified as a result of the long range correlation effects for large and weak fluctuations. The statistical analysis of spectral parameters with the nonparametric Wilcoxon test distinguish state  $D_3$  (6 month after the surgery). There were statistically significant differences between  $D_3$  and the rest of stages for the spectrum width in the case of both detrending methods – DFA and EMD. Applied fractal methods also show the decreasing width and spectrum maximum one month after the surgical operation for all of the patients. The differences are small but the tendency is visible. The findings reflect also the visual variety of the raw data between the stage  $D_2$  and all others.

Conflicts of Interest: None

Funding: This work was partially supported by the JUMC research grant: K/ZDS/006369.

Ethical Approval: Research was approved by a decision of Bioethical Committee of Jagiellonian University for research grant WL-ZKL-94.

## References

- [1] M. Nowakowski, K. A. Tomaszewski, R. M. Herman, J. Sałowka, M. Romaniszyn, M. Rubinkiewicz, J. A. Walocha, Developing a new electromyography-based algorithm to diagnose the etiology of fecal incontinence, International journal of colorectal disease 29 (6) (2014) 747–754.



- [2] R. Merletti, A. Bottin, C. Cescon, D. Farina, M. Gazzoni, S. Martina, L. Mesin, M. Pozzo, A. Rainoldi, P. Enck, Multichannel surface emg for the non-invasive assessment of the anal sphincter muscle, *Digestion* 69 (2) (2004) 112–122.
- [3] F. Bray, A. Jemal, N. Grey, J. Ferlay, D. Forman, Global cancer transitions according to the human development index (2008–2030): a population-based study, *The lancet oncology* 13 (8) (2012) 790–801.
- [4] P. Enck, H. Hinninghofen, R. Merletti, F. Azpiroz, The external anal sphincter and the role of surface electromyography, *Neurogastroenterology & Motility* 17 (s1) (2005) 60–67.
- [5] D. W. Kauff, N. Wachter, A. Heimann, T. B. Kruger, K. P. Hoffmann, H. Lang, W. Kneist, Surface Electromyography Reliably Records Electrophysiologically Evoked Internal Anal Sphincter Activity: A More Minimally Invasive Approach for Monitoring Extrinsic Innervation, *Eur Surg Res* 57 (1-2) (2016) 81–88.
- [6] C. Cescon, L. Mesin, M. Nowakowski, R. Merletti, Geometry assessment of anal sphincter muscle based on monopolar multichannel surface EMG signals, *J Electromyogr Kinesiol* 21 (2) (2011) 394–401.
- [7] A. López, B. Y. Nilsson, A. Mellgren, J. Zetterström, B. Holmström, Electromyography of the external anal sphincter, *Diseases of the colon & rectum* 42 (4) (1999) 482–485.
- [8] E. Clancy, E. L. Morin, R. Merletti, Sampling, noise-reduction and amplitude estimation issues in surface electromyography, *Journal of Electromyography and Kinesiology* 12 (1) (2002) 1–16.
- [9] M. Lei, Z. Wang, Z. Feng, Detecting nonlinearity of action surface emg signal, *Physics Letters A* 290 (5) (2001) 297–303.
- [10] A. L. Goldberger, L. A. Amaral, J. M. Hausdorff, P. C. Ivanov, C.-K. Peng, H. E. Stanley, Fractal dynamics in physiology: alterations with disease and aging, *Proceedings of the National Academy of Sciences* 99 (suppl 1) (2002) 2466–2472.
- [11] C. Atupelage, H. Nagahashi, M. Yamaguchi, M. Sakamoto, A. Hashiguchi, Multifractal feature descriptor for histopathology, *Analytical Cellular Pathology* 35 (2) (2012) 123–126.
- [12] G. Wang, X.-m. Ren, L. Li, Z.-z. Wang, Multifractal analysis of surface emg signals for assessing muscle fatigue during static contractions, *Journal of Zhejiang University-Science A* 8 (6) (2007) 910–915.
- [13] J. W. Kantelhardt, S. A. Zschiegner, E. Koscielny-Bunde, S. Havlin, A. Bunde, H. E. Stanley, Multifractal detrended fluctuation analysis of nonstationary time series, *Physica A: Statistical Mechanics and its Applications* 316 (1) (2002) 87–114.
- [14] D. Makowiec, A. Rynkiewicz, R. Gałaska, J. Wdowczyk-Szulc, M. Żarczyńska-Buchowiecka, Reading multifractal spectra: aging by multifractal analysis of heart rate, *EPL (Europhysics Letters)* 94 (6) (2011) 68005.
- [15] J. Gierałowski, J. Żebrowski, R. Baranowski, Multiscale multifractal analysis of heart rate variability recordings with a large number of occurrences of arrhythmia, *Physical Review E* 85 (2) (2012) 021915.
- [16] A. O. Andrade, S. Nasuto, P. Kyberd, C. M. Sweeney-Reed, F. Van Kanijn, Emg signal filtering based on empirical mode decomposition, *Biomedical Signal Processing and Control* 1 (1) (2006) 44–55.
- [17] D. Liu, M. Luo, Q. Fu, Y. Zhang, K. M. Imran, D. Zhao, T. Li, F. M. Abrar, Precipitation complexity measurement using multifractal spectra empirical mode decomposition detrended fluctuation analysis, *Water Resources Management* (2015) 1–18.
- [18] J.-R. Yeh, S.-Z. Fan, J.-S. Shieh, Human heart beat analysis using a modified algorithm of detrended fluctuation analysis based on empirical mode decomposition, *Medical engineering & physics* 31 (1) (2009) 92–100.
- [19] X.-Y. Qian, G.-F. Gu, W.-X. Zhou, Modified detrended fluctuation analysis based on empirical mode decomposition for the characterization of anti-persistent processes, *Physica A: Statistical Mechanics and its Applications* 390 (23) (2011) 4388–4395.
- [20] C.-K. Peng, S. V. Buldyrev, S. Havlin, M. Simons, H. E. Stanley, A. L. Goldberger, Mosaic organization of dna nucleotides, *Physical review e* 49 (2) (1994) 1685.
- [21] E. Rodriguez, J. C. Echeverria, J. Alvarez-Ramirez, Detrended fluctuation analysis of heart intrabeat dynamics, *Physica A: Statistical Mechanics and its Applications* 384 (2) (2007) 429–438.

- [22] J. L. Semmlow, B. Griffel, Biosignal and medical image processing, CRC press, 2014.
- [23] Z. Wu, N. E. Huang, Ensemble empirical mode decomposition: a noise-assisted data analysis method, *Advances in adaptive data analysis* 1 (01) (2009) 1–41.
- [24] M. E. Torres, M. A. Colominas, G. Schlotthauer, P. Flandrin, A complete ensemble empirical mode decomposition with adaptive noise, in: *2011 IEEE International Conference on Acoustics, Speech and Signal Processing (ICASSP)*, IEEE, 2011, pp. 4144–4147.
- [25] P. Caraiani, Evidence of multifractality from emerging european stock markets, *PloS one* 7 (7) (2012) e40693.
- [26] J. W. Kantelhardt, Fractal and multifractal time series, in: *Mathematics of complexity and dynamical systems*, Springer, 2012, pp. 463–487.
- [27] E. A. Ihlen, Introduction to multifractal detrended fluctuation analysis in matlab, *Fractal Analyses: Statistical And Methodological Innovations And Best Practices* (2012) 97.
- [28] H. Salat, R. Murcio, E. Arcaute, Multifractal methodology, *Physica A: Statistical Mechanics and its Applications*.
- [29] G. G. Delaini, M. Scaglia, G. Colucci, L. Hultén, Functional results of sphincter-preserving operations for rectal cancer, in: *Rectal Cancer*, Springer, 2005, pp. 147–155.
- [30] D. Horvatic, H. E. Stanley, B. Podobnik, Detrended cross-correlation analysis for non-stationary time series with periodic trends, *EPL (Europhysics Letters)* 94 (1) (2011) 18007.